AD 731041

NUSC Report No. 4103

Fast Field Program for Multilayered Media

FREDERICK R. DINAPOLI
Computer Laboratory

DDC
RECEIVED
OCT 18 1971
B

26 August 1971

NAVAL UNDERWATER SYSTEMS CENTER
Newport, Rhode Island 02840

Approved for public release, distribution unlimited.

Reproduced by
NATIONAL TECHNICAL
INFORMATION SERVICE
Springfield, Va. 22151

ABSTRACT

The Fast Field Program (FFP) is a technique for applying Fast Fourier Transform methods to Field theory. Interim results are presented for the FFP as it would be applied to a multilayered ocean. Earlier work on this subject has demonstrated the accuracy of the approach, but a reduction in computing time was needed to attain "real time," in situ propagation estimations. A step in this direction has been made possible by the assumption that the water column is subdivided into strata within which the velocity of sound is allowed to vary exponentially with depth. The kernel of the integral expression for the pressure field is then given in terms of products of cylindrical functions, which can be calculated rapidly through the utilization of recurrence relations. Comparisons of the results of the FFP and normal mode theory are provided for both a shallow and a deep water example at low acoustic frequencies. In the latter case, consideration is given to the influence of the subbottom structure upon propagation predictions. The technique described is not the ultimate solution for real time calculations; however, it does represent the fastest possible version of generating FFP predictions known to the author at this time.

ADMINISTRATIVE INFORMATION

This research was conducted under NUSC Project No. 1A616-50-00, "TUBA II Concurrent Evaluation," Principal Investigator, C. D. Mason (Code SA1), and Navy Subproject and Task No. S 3601-14912, Program Manager, C. Shippey, NAVSHIPS (Code PMS-385).

Portions of this report were presented orally at the "NUSC 2nd In-House ASW Modeling and Simulation Seminar," held at NUSC on 10-11 February 1971.

The Technical Reviewer for this report was Dr. G. A. Leibiger (Code PA3).

ACCESSION for
CFSTI WHITE SECTION
DDC BUFF SECTION
UNANNOUNCED
JUSTIFICATION
BY
DISTRIBUTION/AVAILABILITY CODES
DIST. AVAIL. and/or SPECIAL
A

REVIEWED AND APPROVED: 26 August 1971

G. M. Milligan
Director of Engineering

Inquiries concerning this report may be addressed to the author via Officer in Charge, New London Laboratory, Naval Underwater Systems Center, New London, Connecticut 06320

UNCLASSIFIED

Security Classification

DOCUMENT CONTROL DATA - R & D

Security classification of title, body of abstract and indexing annotation must be entered when the overall report is classified)

1. ORIGINATING ACTIVITY (Corporate author) Naval Underwater Systems Center Newport, Rhode Island 02840	2a. REPORT SECURITY CLASSIFICATION UNCLASSIFIED 2b. GROUP

3. REPORT TITLE

FAST FIELD PROGRAM FOR MULTILAYERED MEDIA

4. DESCRIPTIVE NOTES (Type of report and inclusive dates)

Research Report

5. AUTHOR(S) (First name, middle initial, last name)

Frederick R. DiNapoli

6. REPORT DATE 26 August 1971	7a. TOTAL NO. OF PAGES 40	7b. NO. OF REFS 11
8a. CONTRACT OR GRANT NO b. PROJECT NO 1A616-50-00 c. S3601-14912 d.	9a. ORIGINATOR'S REPORT NUMBER(S) 4103 9b. OTHER REPORT NO(S) (Any other numbers that may be assigned this report)	

10. DISTRIBUTION STATEMENT

Approved for public release; distribution unlimited.

11. SUPPLEMENTARY NOTES	12. SPONSORING MILITARY ACTIVITY Department of the Navy

13. ABSTRACT

The Fast Field Program (FFP) is a technique for applying Fast Fourier Transform methods to Field theory. Interim results are presented for the FFP as it would be applied to a multilayered ocean. Earlier work on this subject has demonstrated the accuracy of the approach, but a reduction in computing time was needed to attain "real time," in situ propagation estimations. A step in this direction has been made possible by the assumption that the water column is subdivided into strata within which the velocity of sound is allowed to vary exponentially with depth. The kernel of the integral expression for the pressure field is then given in terms of products of cylindrical functions, which can be calculated rapidly through the utilization of recurrence relations. Comparisons of the results of the FFP and normal mode theory are provided for both a shallow and a deep water example at low acoustic frequencies. In the latter case, consideration is given to the influence of the subbottom structure upon propagation predictions. The technique described is not the ultimate solution for real time calculations; however, it does represent the fastest possible version of generating FFP predictions known to the author at this time.

DD FORM 1 NOV 65 1473 (PAGE 1)

S/N 0102-014-6600

UNCLASSIFIED

Security Classification

UNCLASSIFIED
Security Classification

14 KEY WORDS	LINK A ROLE	LINK A WT	LINK B ROLE	LINK B WT	LINK C ROLE	LINK C WT
Fast Field Program						
Fast Fourier Transform						
Normal Mode Theory						

DD FORM 1 NOV 65 1473 (BACK)
(PAGE 2)

UNCLASSIFIED
Security Classification

TABLE OF CONTENTS

	Page
LIST OF TABLES	iii
LIST OF ILLUSTRATIONS	iii
INTRODUCTION	1
THE FAST FIELD PROGRAM (FFP) AND THE FAST FOURIER TRANSFORM (FFT)	1
STRUCTURING OF THE KERNEL FOR THE RAPID CALCULATION OF THE INPUT	3
THE SINGLE EXPONENTIAL LAYER	5
The Green's Function	7
Sampling the Input	8
Comparison of the FFP and Normal Mode Theory	9
THE TWO-LAYER MODEL	13
The Green's Function	16
Multilayers and Sampling	18
Comparison of the FFP and Normal Mode Theory	21
DISCUSSION	34
REFERENCES	37
INITIAL DISTRIBUTION LIST	Inside Back Cover

LIST OF TABLES

Table		Page
1	Variables and Required Locations	20

LIST OF ILLUSTRATIONS

Figure		
1	Environmental Description for a Single Exponential Layer	6
2	Magnitude of Input for the Single Exponential Layer	10
3	Comparison of FFP and Normal Mode Predictions: Single Layer	11
4	Total FFP Results for the Single Exponential Layer	12
5	Environmental Description for the Tyrrhenian Sea	14
6	Hastrup's Bottom Loss Measurements for the Tyrrhenian Sea	15
7	Theoretical Bottom Loss for the Tyrrhenian Sea	16
8	Staggered Start for the Multilayer Case	19
9	FFP Propagation Loss for a Semi-infinite Bottom and a Frequency of 25 Hz	23
10	FFP Propagation Loss for a Two-layered Bottom and a Frequency of 25 Hz	24
11	FFP Propagation Loss for a Two-layered Bottom and a Frequency of 35 Hz	26
12	FFP Propagation Loss for a Two-layered Bottom and a Frequency of 50 Hz	27
13	FFP Propagation Loss for a Two-layered Bottom and a Frequency of 100 Hz	28
14	FFP Propagation Loss for a Semi-infinite Bottom and a Frequency of 100 Hz	29
15	Comparison of Input at 35 Hz for Different Bottom Structures	30-33

FAST FIELD PROGRAM FOR MULTILAYERED MEDIA

INTRODUCTION

The capability to provide "real time," in situ propagation predictions is highly desirable in many diverse areas of underwater acoustics. It is precisely this wide diversity, however, that makes it difficult to define what real time is. The philosophy employed here is to develop the fastest possible method of providing estimations and let the eventual user make the decision regarding time for his particular application.

The previous work[1,2] on the Fast Field Program (FFP), a technique of applying Fast Fourier Transform (FFT) methods to Field theory, has clearly demonstrated the soundness of the concept and the accuracy of the predictions. In this earlier work, two schemes were investigated for generating the input data to be transformed. The first involved a numerical integration of the depth dependent differential equation for an arbitrary sound velocity profile. In the second approach, the variation of the sound velocity with depth was restricted in such a way that known solutions were available. Intrinsic difficulties of the same type were found for both methods, and it was felt that the required computing time could be reduced. The technique described in this report offers such a reduction.

THE FAST FIELD PROGRAM (FFP) AND THE FAST FOURIER TRANSFORM (FFT)

It is well known[2] that the field due to a monochromatic point source can be represented as

$$\psi(z,r) = \int_{-\infty}^{\infty} G(z,z_s;\xi)\, H_0^{(1)}(\xi r)\, \xi\, d\xi \,. \tag{1}$$

The scalar, ψ, is related to the pressure field and the particle velocity through the expressions

$$P = \rho^{1/2}\, \psi(z,r)$$

$$V = \frac{1}{i\omega\rho} \nabla P, *$$

where ρ is an abbreviation for the density. The function G represents the depth dependent Green's function, which must simultaneously satisfy

$$\frac{d^2\beta}{dz^2} + \left[k^2(z) - \xi^2\right] \beta = - \delta(z-z_s) \tag{2}$$

and associated boundary conditions where z_s is the depth of the source.

Let the Hankel function in Eq. (1) be approximated by the first term in its asymptotic expansion,

$$H_0^{(1)}(\xi r) \cong \left(\frac{2}{\pi i}\right)^{1/2} (\xi r)^{-1/2} e^{i\xi r} ,$$

and simultaneously let the variables, ξ and r, be approximated according to

$$\xi_m = \xi_0 + m\Delta\xi$$

$$r_n = r_0 + n\Delta r \qquad (n,m) = 0,1,2,\cdots,N-1, \tag{3}$$

with the added restriction that

$$\Delta r \, \Delta\xi = \frac{2\pi}{N} .$$

The value of N is 2 raised to some integer power. Equation (1) is then given by the discrete Fourier transform

$$\psi(z,r_n) \cong \Delta\xi\left(\frac{2}{\pi i}\right)^{1/2} \frac{e^{i\xi_0 r_n}}{r_n^{1/2}} \sum_{m=0}^{N-1} E_m \, e^{i2\pi mn/N} , \tag{4}$$

---

* A time variation of $e^{i\omega t}$ will be uniformly suppressed throughout the analysis.

and the input to the FFT is found to be

$$E_m = G(z, z_s; \xi_m)\, \xi_m^{1/2}\, e^{imr_0\Delta\xi} \quad . \tag{5}$$

Equation (4) is now in a form that is directly amenable to the FFT.[3] The result of the application of the FFT is the value of the field at each of the discrete N ranges. Once the input, Eq. (5), is obtained, the calculation of Eq. (4) proceeds very rapidly. For the UNIVAC 1108 and N = 8192, this calculation consumes 2.689 sec. The main concern of this report is with the rapid calculation of accurate values of the input. The basis of a scheme that allows this to be done is discussed in the next section.

STRUCTURING OF THE KERNEL FOR THE RAPID CALCULATION OF THE INPUT

The wave number, $k = \sqrt{(\omega/c_j)^2 + 2i\alpha}$, in Eq. (2) is assumed to be a complex with attenuation coefficient $\alpha > 0$ since the Green's functions could be singular along the axis of integration. The homogeneous form of Eq. (2) is then written as

$$\frac{d^2\beta_j}{dz^2} + \left[\frac{\omega^2}{c_j^2(z)} - (\xi^2 - 2i\alpha)\right]\beta_j = 0 \qquad z_j \le z \le z_{j+1} \; . \tag{6}$$

The subscript j is included in anticipation of the subdivision of the velocity profile into strata. In order to provide insight into the motivation for this subdivision, a slight digression is necessary.

The general solution of Eq. (6) for an arbitrary sound velocity profile can be obtained by numerical integration. Two linearly independent solutions can be obtained for a given value of ξ_m; these solutions satisfy the relevant boundary conditions and thus allow the construction of the Green's function. These solutions change their character at the turning point. The transition from an oscillatory to an exponential behavior, or vice versa, can be extremely sensitive to round-off errors for certain profiles. At the same time, the solutions exhibiting a turning point as a function of ξ_m with z fixed are the most important contributors to the integration in Eq. (1). It is certainly true that the accuracy of the process may be improved by resorting to double precision or special integration techniques. The price paid for these manipulations, how-

ever, is additional computer time. Even if one were to ignore this aspect of the problem, the prospect still remains that the integration must be repeated for each of the N discrete values of ξ_m. The result is that the amount of computer time needed to generate the input is unsatisfactory when compared with the time required to do the FFT.

If the variation of the profile is restricted, known solutions of Eq. (6) are available. This approach was utilized[2] by fixing the value of the profile at three arbitrary points, and the solutions were given in terms of hypergeometric functions. This technique has essentially the same limitations as numerical integration. As the frequency or water depth is increased, there is a corresponding increase in the required computing time and in the difficulty with round-off errors. As was mentioned earlier, when speed is not the prime concern the problem of round-off errors can usually be circumvented, and thus the above-mentioned approaches are possible candidates for the generation of the input.

To return to the technique of this report, let the profile be restricted to vary exponentially with depth within each layer according to

$$c_j(z_i) = c_{j-1}(z_1)\, e^{\pm(z_i - z_j)/H_j} \qquad z_j \le z_i \le z_{j+1} \quad ,$$

where $j = 1, 2, \cdots$, and $c_0(z_1)$ is the surface velocity. The z axis is taken to be positive in the downward direction. The solutions of Eq. (6) are then found to be

$$\beta_j(z_i) = C_{\nu_j}\left[\gamma_j^i(z_i)\right] , \tag{7}$$

that is, in terms of cylindrical functions of complex order

$$\nu_j \cong (\xi H_j - i\alpha H_j) \tag{8}$$

and real argument

$$\gamma_j^i(z_i) = \frac{\omega H_j}{c_{j-1}(z_j)}\, e^{\pm(z_i - z_j)/H_j} \quad . \tag{9}$$

The possible values of z_i are either one of the interface depths or the source or receiver depths.

The variation of G as a function of ξ may now be obtained economically and rapidly through the recurrence relations for products of cylindrical functions. This aspect of the technique will be given more detailed attention in the next section. The fact that the input can now be obtained by utilization of a recurrence relation is most desirable, but it does not complete the requirements. The recurrence relation must also be linear in the variable ξ since the samples in the FFT need be equispaced. One other profile that meets these specifications is known to the author. Consider the equation

$$\frac{d^2\beta}{dz^2} + \left[\frac{\nu(\nu+1)}{H^2 \cosh^2\left(\frac{z - z_1}{H}\right)} - \left(\frac{\mu}{H}\right)^2\right]\beta = 0 .$$

The basis of solutions is found to be

$$\beta_1(z) = P_\nu^\mu\left[\tanh\left(\frac{z - z_1}{H}\right)\right]$$

$$\beta_2(z) = Q_\nu^\mu\left[\tanh\left(\frac{z - z_1}{H}\right)\right] , \tag{10}$$

and the desired recurrence relation,[4] satisfied by both of the solutions in Eq. (10), is

$$P_\nu^{\mu+2}(x) + 2(\mu+1)\frac{x}{\sqrt{1-x^2}}P_\nu^{\mu+1}(x) + (\nu-\mu)(\nu+\mu+1)P_\nu^\mu(x) = 0 .$$

The cosh profile of the associated Legendre functions, Eq. (10), is not significantly different from the exponential profile; thus, it was decided to use the cylindrical functions.

THE SINGLE EXPONENTIAL LAYER

The case that requires the least amount of computer time is that in which the velocity profile can be represented by a single exponential layer, as depicted in Fig. 1. The bottom was assumed to be a homogeneous liquid, semi-infinite in extent, and with a velocity faster than that of the overlying water. The densities of the water and bottom were taken to be identical for convenience.

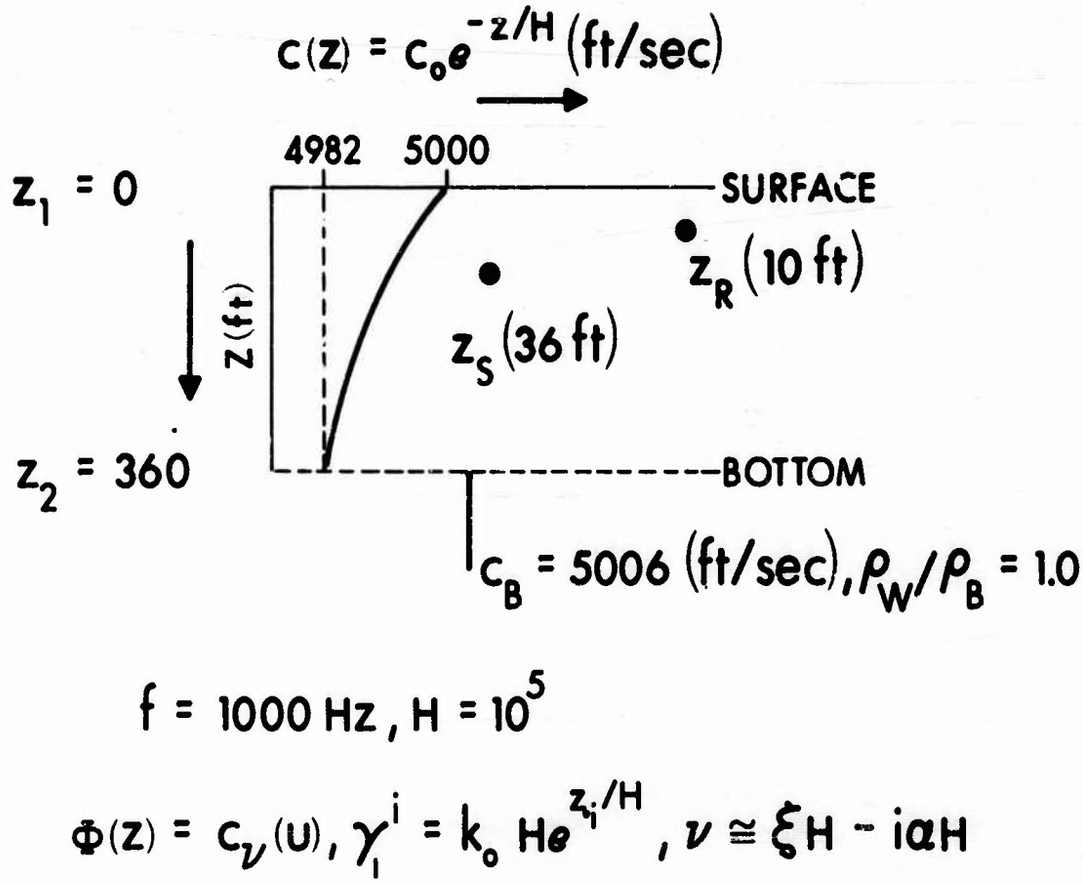

$$f = 1000\ \text{Hz},\ H = 10^5$$

$$\Phi(z) = c_\nu(U),\ \gamma_1^i = k_0 H e^{z_i/H},\ \nu \cong \xi H - i\alpha H$$

Fig. 1. Environmental Description for a Single Exponential Layer

It is faster, from a computational point of view, to allow the velocity in the bottom to also vary exponentially with depth. The information could then be obtained from a recurrence relation rather than the evaluation of a square root of a complex number and a trigonometric function for each of the N values of ξ_m. The normal mode program that was employed for comparison purposes, however, could not accommodate such a structure.

THE GREEN'S FUNCTION

The constituents of the Green's function[5] are found to be

$$G(z_r, z_s; \xi) = \begin{cases} \left(\frac{\pi H}{2}\right) P_\nu(\gamma_1^1, \gamma_1^r) \dfrac{\left[Q_\nu(\gamma_1^s, \gamma_1^2) - Y_2^2 P_\nu(\gamma_1^s, \gamma_1^2)\right]}{\left[Q_\nu(\gamma_1^1, \gamma_1^2) - Y_2^2 P_\nu(\gamma_1^1, \gamma_1^2)\right]} & z_1 \le z_r \le z_s \\ \left(\frac{\pi H}{2}\right) P_\nu(\gamma_1^1, \gamma_1^s) \dfrac{\left[Q_\nu(\gamma_1^r, \gamma_1^2) - Y_2^2 P_\nu(\gamma_1^r, \gamma_1^2)\right]}{\left[Q_\nu(\gamma_1^1, \gamma_1^2) - Y_2^2 P_\nu(\gamma_1^1, \gamma_1^2)\right]} & z_s \le z_r \le z_2 , \end{cases}$$

where the products of cylindrical functions are defined as

$$\begin{aligned} P_\nu(a,b) &= J_\nu(a)\, Y_\nu(b) - J_\nu(b)\, Y_\nu(a) \\ Q_\nu(a,b) &= J_\nu(a)\, Y_\nu'(b) - J_\nu'(b)\, Y_\nu(a) \\ R_\nu(a,b) &= J_\nu'(a)\, Y_\nu(b) - J_\nu(b)\, Y_\nu'(a) \\ S_\nu(a,b) &= J_\nu'(a)\, Y_\nu'(b) - J_\nu'(b)\, Y_\nu'(a) . \end{aligned} \tag{11}$$

The primes will always denote differentiation with respect to the argument. The last two expressions of Eq. (11) are not needed explicitly for this example but will be required in the next section. The admittance of the bottom, Y_2^2, is found to be

$$Y_2^2 = \begin{cases} i\sqrt{(\omega/c_B)^2 - \xi^2}\Big/\gamma_1^2 & |\xi| < \omega/c_B \\ -\sqrt{\xi^2 - (\omega/c_B)^2}\Big/\gamma_1^2 & |\xi| > \omega/c_B . \end{cases}$$

The representation for the Green's function in terms of the products of cylindrical functions, Eq. (11), is not only symbolically efficient but it also represents a savings in computing time. These products can be evaluated rapidly through the recurrence relations,[6, 7]

$$Q_{\nu+1} = - R_\nu + (\nu/a)\, P_\nu - \frac{(\nu+1)}{b}\, P_{\nu+1}$$

$$R_{\nu+1} = - Q_\nu + (\nu/b)\, P_\nu - \frac{(\nu+1)}{a}\, P_{\nu+1}$$

$$P_{\nu+2} = P_\nu - 2\,(\nu+1)\left[Q_{\nu+1}/a + R_{\nu+1}/b\right]$$

$$S_{\nu+1} = P_{\nu+2} + (\nu+1)\left[Q_{\nu+1}/a + R_{\nu+1}/b\right] - \frac{(\nu+1)^2}{ab}\, P_{\nu+1}\,. \tag{12}$$

Two areas of concern associated with Eq. (12) are the availability of starting values and the stability of the recurrence process. For the examples examined, the WKB approximations of the functions defined in Eq. (11) provide accurate starting values. The question of stability is most important when the value of the real part of ν lies between the arguments a and b. The difference between these arguments increases with either increasing frequency or water depth. The behavior of the functions in Eq. (11) within this transition region takes the form of an oscillatory function modulated by a growing exponential envelope. As this separation distance increases, the envelope grows proportionally and thereby enhances the possibility that round-off error will affect the calculations of Eq. (12). A more detailed account of these aspects and a method of overcoming the latter is provided in Reference 8.

SAMPLING THE INPUT

The sampling distance in the wave number domain is determined by the scaling factor H and the fact that the change in ν must be unity. Then from Eq. (8) one sees that

$$\Delta\xi = \frac{1}{H}\,. \tag{13}$$

The magnitude of H for most applications will be on the order of 10^5. The sampling distance, Eq. (13), may be too coarse at some frequencies; however,

it may be altered as will be explained in the section on the two-layer model. The parameter α is assigned the value of the attenuation coefficient at the frequency of interest. The sampling region should encompass that portion of the real ξ axis near the region in which the Green's function is singular. If k_{max} is the wave number corresponding to the minimum velocity of the water-bottom combination, the beginning of the sampling region is found from

$$\xi_0 = k_{max} - N\Delta\xi \ . \tag{14}$$

The integrand decays to zero for values of ξ greater than k_{max}. The selection of N then determines the length of the axis sampled. The question of how large N must be is the analog of how many modes one includes in normal mode theory. It is worth emphasizing that the FFP is <u>not</u> an eigenvalue problem. It is not necessary to know the exact location of the singularities in the complex ξ plane, but rather only the bounds of the region where they are distributed. Certain crude but useful techniques are available to answer questions regarding $\Delta\xi$ and N. The value of $\Delta\xi$ can be doubled and N reduced to one-half of its previous value. In this way the length of the region sampled, $N\Delta\xi$, is unchanged and the effect of a smaller sampling distance can be determined. A doubling of N with $\Delta\xi$ unchanged will show the significance of effectively adding more modes.

COMPARISON OF THE FFP AND NORMAL MODE THEORY

One method to demonstrate the relationship between the FFP and normal mode theory is to examine the magnitude of the input as a function of the wave number. This information is presented in Fig. 2 for the problem under consideration. The series of peaks is the result of nearby singularities of the Green's function, which would give rise to the normal modes. The numbers associated with these peaks are the mode numbers derived by Bartberger and Ackler by using their three-layer, normal mode program.[9] In all, they calculated 37 modes with their last eigenvalue having a real part of 1.217. Excellent agreement was found between the location of the peaks and the real part of their eigenvalues. As can be seen, the region sampled by the FFP includes more of the high-order modes but omits the first four low-order modes.

Propagation loss versus range is displayed in Fig. 3. The upper graph represents the normal mode predictions and the lower graph represents that of the FFP. The range resolution for the FFP was four times as small as that used in the normal mode program, and this fact accounts for the greater detail

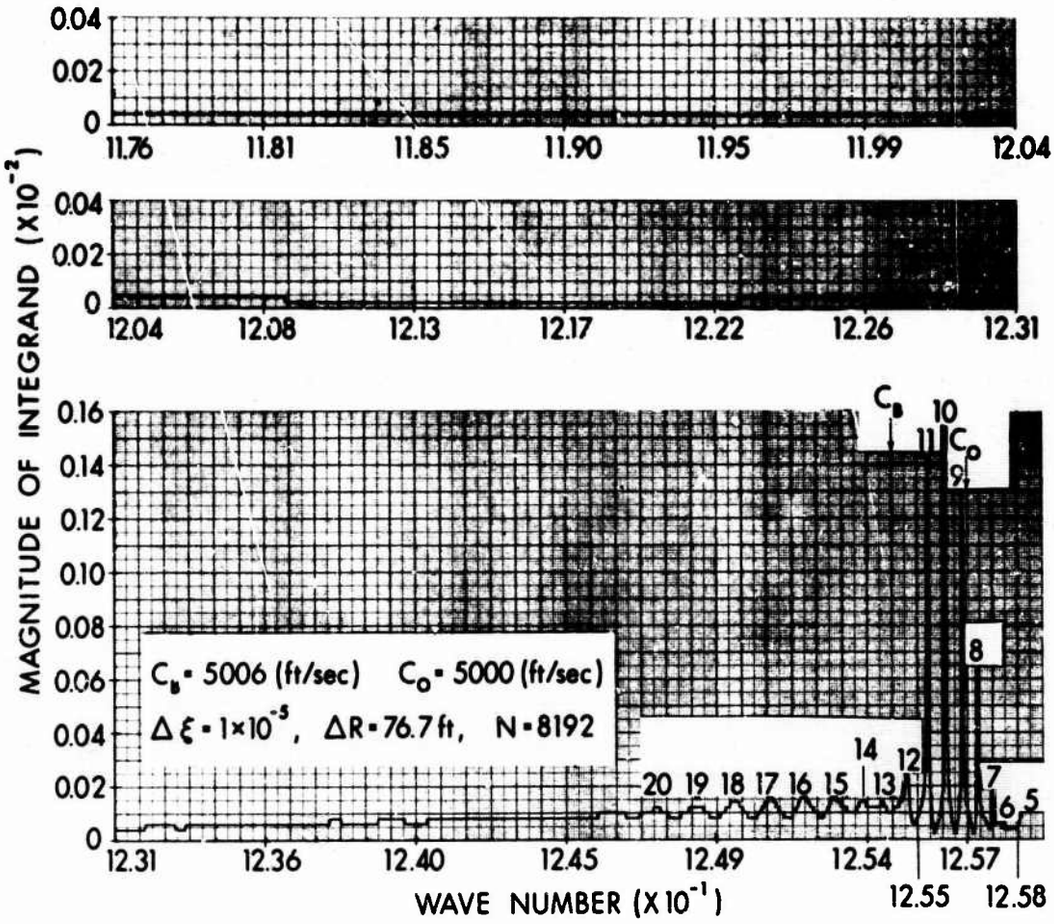

Fig. 2. Magnitude of Input for the Single Exponential Layer

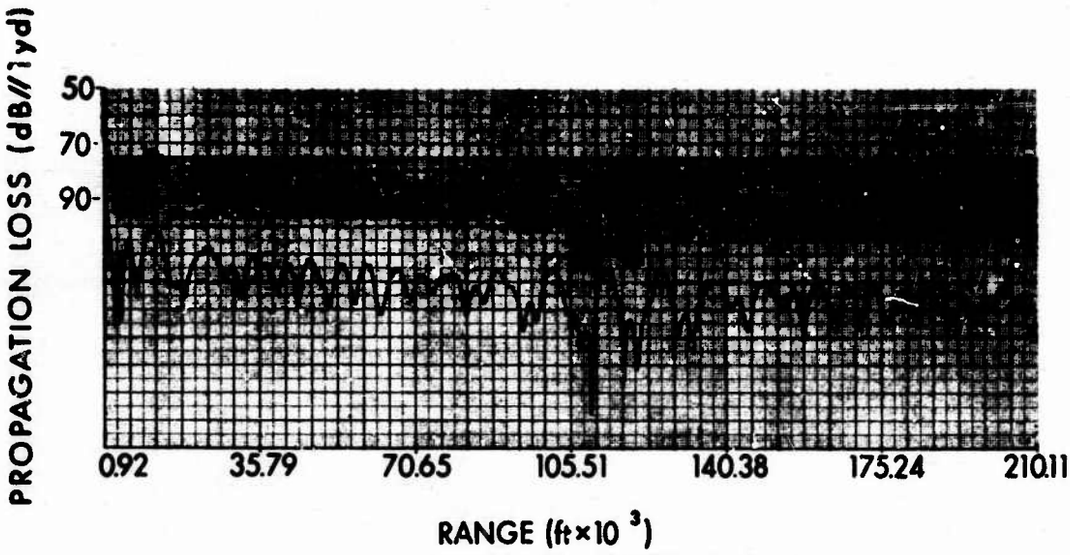

Fig. 3. Comparison of FFP and Normal Mode Predictions: Single Layer

in that pattern. At those points where the ranges of both solutions coincide, the difference between the solutions is no greater than 1 dB. This is the reason for plotting the two results in a displaced manner. The FFP provides results out to about 200 kyd in increments of 26 yd with the input values given in Fig. 2. The total FFP results are shown in Fig. 4, where the effect of aliasing in the FFT calculations is evident at the longest ranges.

The total execution time for this example was 31 sec on the UNIVAC 1108. The ratio of time needed to generate the input to the time required to actually do the FFT is thus about nine to one. Of all the techniques considered for the generation of the input, the single exponential layer requires the least amount of computing time and is considered to be optimum at this stage in the development.

Unfortunately, a single exponential layer is not a representative environmental model. The possibility of using multilayers does exist, however, and the ramifications of this approach are discussed in the next section.

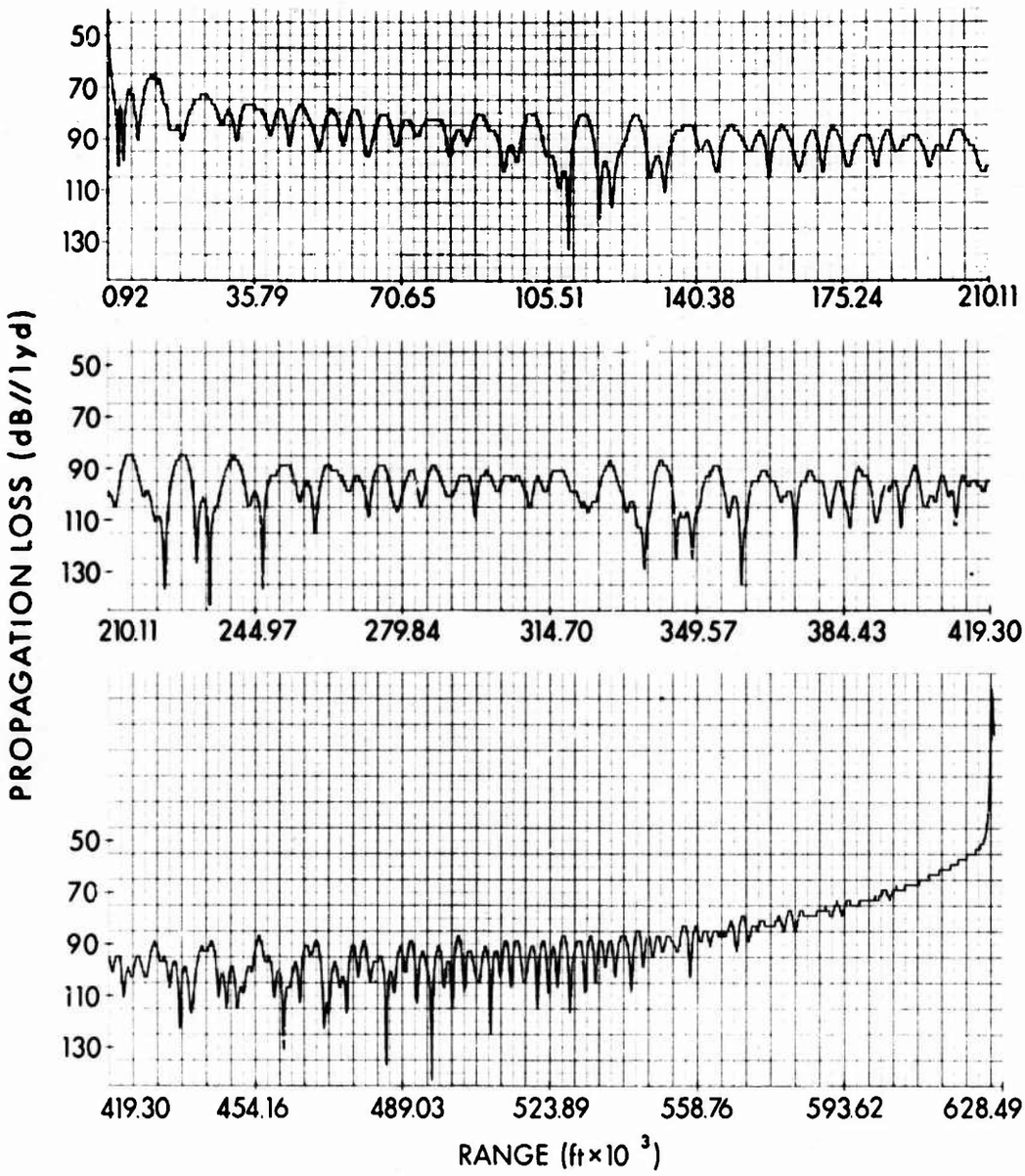

Fig. 4. Total FFP Results for the Single Exponential Layer

THE TWO-LAYER MODEL

A typical warm-weather profile for the Tyrrhenian Sea is given in Fig. 5. The velocity of sound versus depth can be represented by the two exponential layers,

$$c_1(z_i) = c_0(z_1)\, e^{-(z_i - z_1)/H_1} \qquad z_1 \le z_i \le z_2$$

$$c_2(z_i) = c_1(z_2)\, e^{(z_i - z_2)/H_2} \qquad z_2 \le z_i \le z_3 \, .$$

The velocity at the surface, $c_0(z_1)$, was taken to be 5040 ft/sec. The layer depths z_2 and z_3 are 200 and 9000 ft, respectively, and the scaling factors for each layer are

$$H_1 = 12 \times 10^3$$

$$H_2 = 36 \times 10^4 \, .$$

Consideration was given to the subbottom structure, since the frequencies of interest were in the seismic range. The two-layered, liquid bottom finally adopted (Fig. 5) was arrived at by trying to match experimental bottom loss measurements for this area.[10] The results of those measurements are depicted in Fig. 6. The bottom loss in the 75- to 150-Hz band provided by the two-layered bottom is given in Fig. 7. It can be seen that the theoretical curve contains all the important features present in the measurements.

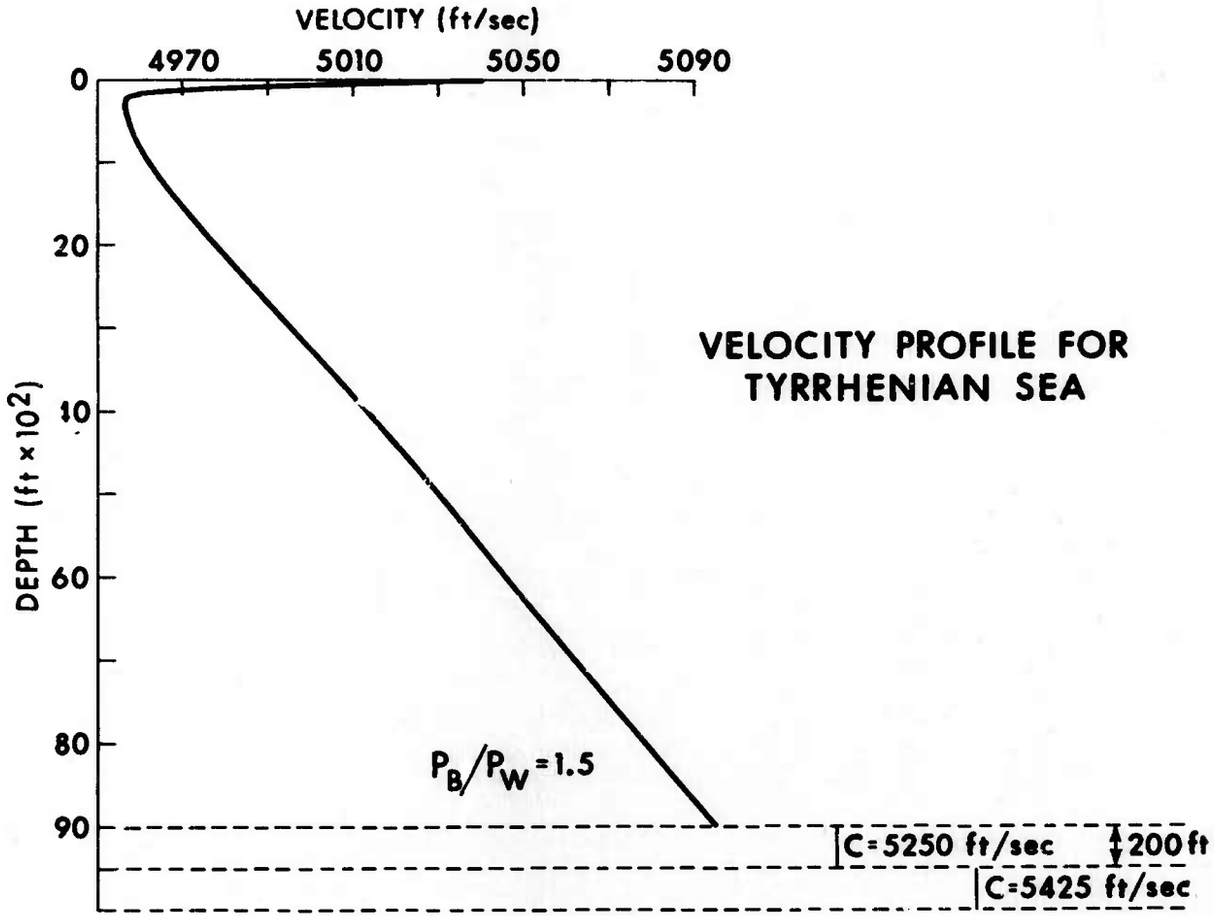

Fig. 5. Environmental Description for the Tyrrhenian Sea

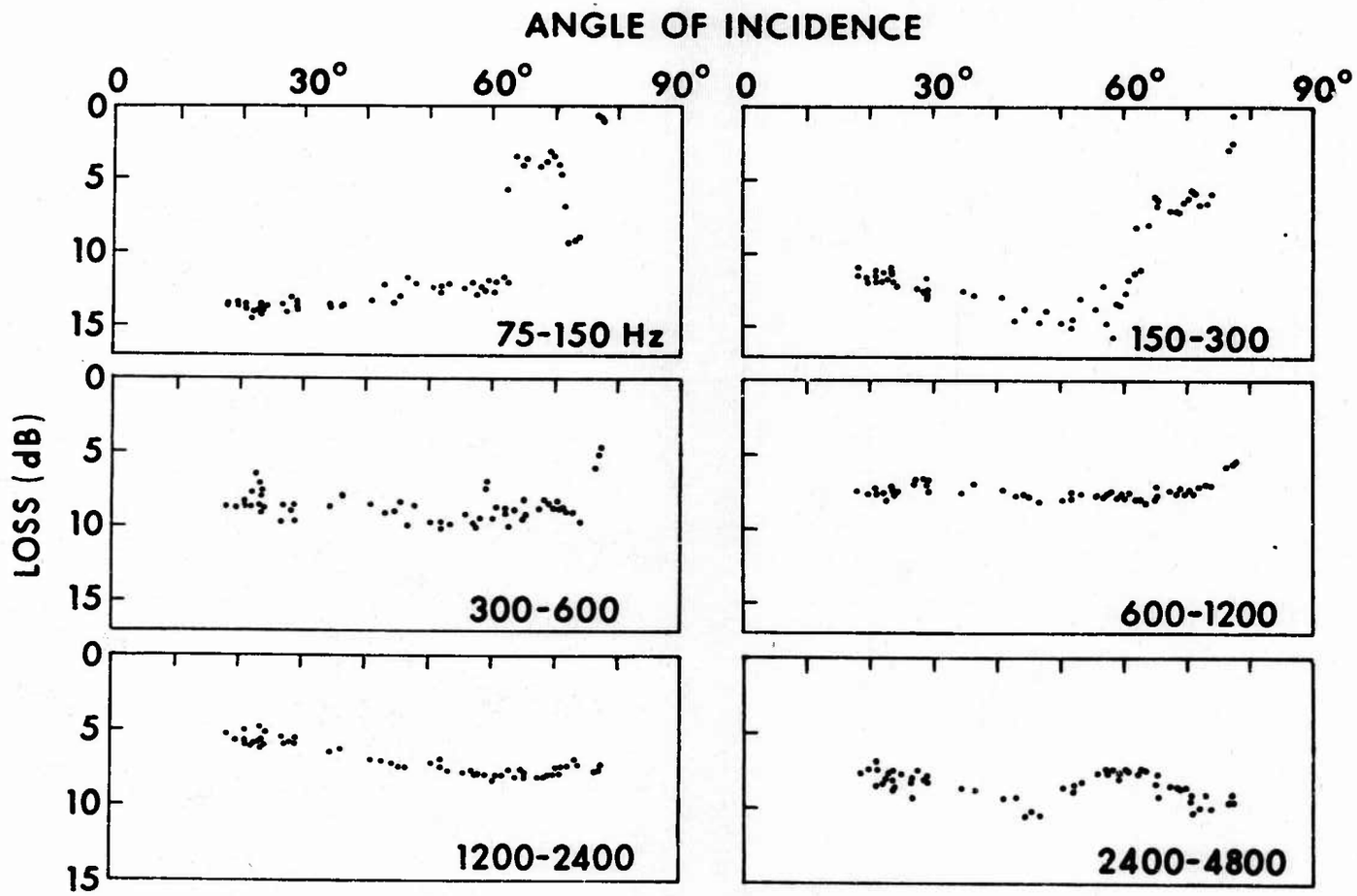

OCTAVE BAND LOSSES

INTEGRATION TIME INCREASED FOR ANGLES OF INCIDENCE LARGER THAN 62°

Fig. 6. Hastrup's Bottom Loss Measurements for the Tyrrhenian Sea

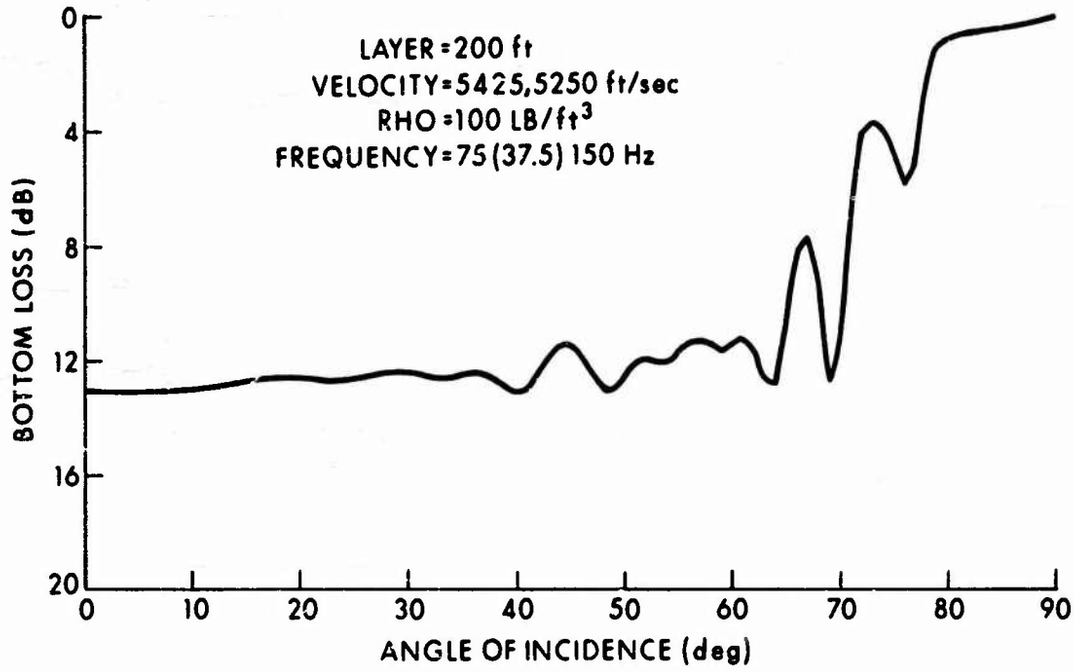

Fig. 7. Theoretical Bottom Loss for the Tyrrhenian Sea

THE GREEN'S FUNCTION

If the same abbreviations introduced in the previous section are utilized, the Green's function, $G(z_s, z_r; \xi)$, for the case of the source in the first layer, is found to be

$$\frac{-\pi H_1}{2} P_{\nu_1}(\gamma_1^1, \gamma_1^r) \frac{\left[\frac{H_1}{\gamma_1^2} Y_2^2 P_{\nu_1}(\gamma_1^s, \gamma_1^2) - Q_{\nu_1}(\gamma_1^s, \gamma_1^2)\right]}{\left[Q_{\nu_1}(\gamma_1^1, \gamma_1^2) - \left(\frac{H_1}{\gamma_1^2}\right) Y_2^2 P_{\nu_1}(\gamma_1^1, \gamma_1^2)\right]} \qquad z_1 \le z_r \le z_s$$

$$\frac{-\pi H_1}{2} P_{\nu_1}(\gamma_1^1, \gamma_1^s) \frac{\left[\frac{H_1}{\gamma_1^2} Y_2^2 P_{\nu_1}(\gamma_1^r, \gamma_1^2) - Q_{\nu_1}(\gamma_1^r, \gamma_1^2)\right]}{\left[Q_{\nu_1}(\gamma_1^1, \gamma_1^2) - \left(\frac{H_1}{\gamma_1^2}\right) Y_2^2 P_{\nu_1}(\gamma_1^1, \gamma_1^2)\right]} \qquad z_s \le z_r \le z_2$$

$$\frac{\frac{H_1}{\gamma_1^2} P_{\nu_1}(\gamma_1^1, \gamma_1^s)\left[\frac{\rho_w}{\rho_B}\left(\frac{-H_2}{\gamma_2^3}\right) Y_3^3 P_{\nu_2}(\gamma_2^r, \gamma_2^3) - Q_{\nu_2}(\gamma_2^r, \gamma_2^3)\right]}{\left[Q_{\nu_1}(\gamma_1^1, \gamma_1^2) - \left(\frac{H_1}{\gamma_1^2}\right) Y_2^2 P_{\nu_1}(\gamma_1^1, \gamma_1^2)\right]\left[\frac{\rho_w}{\rho_B}\left(\frac{-H_2}{\gamma_2^3}\right) Y_3^3 P_{\nu_2}(\gamma_2^2, \gamma_2^3) - Q_{\nu_2}(\gamma_2^2, \gamma_2^3)\right]} \quad z_2 \leq z_r \leq z_3 . \tag{15}$$

The admittance at each of the layer interfaces is

$$Y_2^2 = \left(\frac{-\gamma_2^2}{H_2}\right) \frac{\left[-S_{\nu_2}(\gamma_2^2, \gamma_2^3) + \frac{\rho_w}{\rho_B}\left(\frac{-H_2}{\gamma_2^3}\right) Y_3^3 R_{\nu_2}(\gamma_2^2, \gamma_2^3)\right]}{\left[-Q_{\nu_2}(\gamma_2^2, \gamma_2^3) + \frac{\rho_w}{\rho_B}\left(\frac{-H_2}{\gamma_2^3}\right) Y_3^3 P_{\nu_2}(\gamma_2^2, \gamma_2^3)\right]} \quad z = z_2 \tag{16}$$

$$Y_3^3 = \frac{K_1 \left[K_2 - k_1 \tanh (ik_{z_1} d)\right]}{\left[K_1 - K_2 \tanh (ik_{z_1} d)\right]} \quad z = z_3 , \tag{17}$$

where

$$K_j = \frac{\sqrt{k_j^2 - \xi^2 + 2i\alpha_B}}{(\omega\rho_j)} \quad j = 1,2 \quad ,$$

$$k_{z_1} = \sqrt{k_1^2 - \xi^2 + 2i\alpha_B} \quad ,$$

d is the thickness of the first bottom layer, and subscripts w and B refer to water and bottom, respectively.

MULTILAYERS AND SAMPLING

The addition of multilayers and, thus, different scaling factors provides a choice for the fundamental value of $\Delta\xi$, the sampling distance. The facts that the FFT requires equispaced inputs and that the value of $\Delta\xi$ is different for each layer would seem to be in conflict. This situation can be resolved by setting $\Delta\xi$ equal to the reciprocal of the largest scaling factor and then taking the other scaling factors to be integer multiples of this value. In this instance, one has

$$\Delta\xi = \frac{1}{H_2}, \quad \frac{H_2}{H_1} = 30 .$$

As before, the beginning of the sampling region is found from Eq. (14). The discrete values of the order for each layer are then found to be

$$(\nu_2)_m = (\xi_0 H_2 - i\alpha H_2) + m \tag{18}$$

$$(\nu_1)_m = (\xi_0 H_1 - i\alpha H_1) + m\frac{H_1}{H_2}, \tag{19}$$

since

$$\xi_m = \xi_0 + \frac{m}{H_2},$$

where $m = 0, 1, 2, \cdots, N-1$.

The recurrence relations (Eq. (12)) yield the value of the required functions at successive values of the order which differ by unity. Those values would coincide exactly with the discrete values of Eq. (18) but not those of Eq. (19). The remedy for the latter case is to have H_2/H_1 starting values for the first layer. The relationship between the variable of integration, the order for each layer, and the path through these values when utilizing Eq. (12) is illustrated graphically in Fig. 8. The implication of this process on computer storage is provided in Table 1.

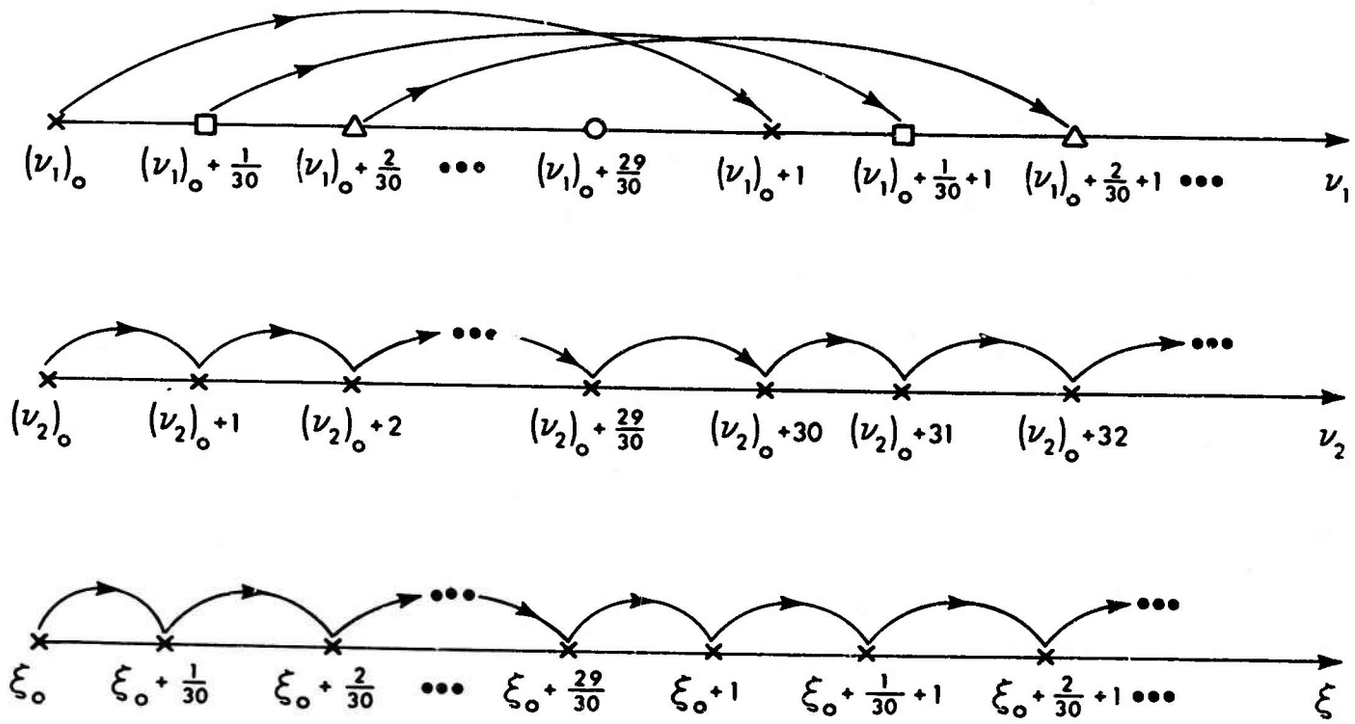

Fig. 8. Staggered Start for the Multilayer Case

Table 1

VARIABLES AND REQUIRED LOCATIONS

Variable	Required Locations (Complex)
P_{ν_1}	2
Q_{ν_1}	1
R_{ν_1}	1
S_{ν_1}	1
P_{ν_2}	60
Q_{ν_2}	30
R_{ν_2}	30
S_{ν_2}	30
$G(z_s, z_r; \xi_m)$	N

It is possible to set $\Delta\xi$ equal to the reciprocal of the smallest scaling factor, calculate Eq. (12) for ν_2 as before, but only retain every thirtieth value. This procedure results in a larger fundamental sampling distance. However, this result is also available with the first scheme. Suppose the smallest fundamental sampling distance is decided upon. If it is desirable to double this value, one would merely have to do twice as many calculations and retain every other

one. On the other hand, the sampling distance can be halved by repeating the procedure outlined in Table 1 twice with $N = N/2$. The second time the starting point would be $\xi_0 = \xi_0 + \Delta\xi/2$.

COMPARISON OF THE FFP AND NORMAL MODE THEORY

The normal mode calculations were performed by Bartberger and Ackler at NADC using their three-layer program. A modification of the program was required to accommodate a multilayered bottom. This was accomplished[11] by retaining only the magnitude of the reflection coefficient at the water bottom. The magnitude of the reflection coefficient was that produced by the two-layered bottom used in the FFP calculations. All normal mode predictions associated with this example were obtained with the above-described reflection coefficient. FFP calculations were performed with the two-layered bottom and with a semi-infinite bottom having the velocity of the second bottom layer. By utilizing both types of bottoms and increasing the frequency while other parameters were held constant, it was hoped that the significance of the subbottom structure could be determined.

A qualitative indication of the influence of the bottom can be obtained from an examination of the Green's function. Consider Eq. (15) for the case when the receiver is in the second layer. The smallest argument of the product functions for the second layer is γ_2^3, since the velocity gradient is positive in this layer. The function $Y_{\nu_2}(\gamma_2^3)$ will eventually dominate these product functions when $|\nu_2| > \gamma_2^3$. At some point in the sampling process one has the approximate values

$$P_{\nu_2}(\gamma_2^2, \gamma_2^3) \cong J_{\nu_2}(\gamma_2^2)\, Y_{\nu_2}(\gamma_2^3)$$

$$Q_{\nu_2}(\gamma_2^2, \gamma_2^3) \cong J_{\nu_2}(\gamma_2^2)\, Y'_{\nu_2}(\gamma_2^3)$$

and, similarly,

$$P_{\nu_2}(\gamma_2^r, \gamma_2^3) \cong J_{\nu_2}(\gamma_2^r)\, Y_{\nu_2}(\gamma_2^3)$$

$$Q_{\nu_2}(\gamma_2^r, \gamma_2^3) \cong J_{\nu_2}(\gamma_2^r)\, Y'_{\nu_2}(\gamma_2^3)\,.$$

Substitution of these expressions into the Green's function produces

$$G(z_s, z_r; \xi_m) \cong \left(\frac{-H_1}{\gamma_1^2}\right) \frac{P_{\nu_1}(\gamma_1^1, \gamma_1^s)}{\left[Q_{\nu_1}(\gamma_1^1, \gamma_1^2) - \left(\frac{H_1}{\gamma_1^2}\right) Y_2^2 P_{\nu_1}(\gamma_1^1, \gamma_1^2)\right]} \frac{J_{\nu_2}(\gamma_1^2)}{J_{\nu_2}(\gamma_2^r)}, \tag{20}$$

where the admittance of the second layer reduces to

$$Y_2^2 \cong \left(\frac{\gamma_2^2}{-H_2}\right) \frac{J'_{\nu_2}(\gamma_2^2)}{J_{\nu_2}(\gamma_2^2)} .$$

This expression is now independent of Y_3^3, and thus the bottom has no influence at these values of ν_2.* When the receiver is in the first layer, a similar reduction of the Green's function is possible. As one might expect, the values of the order for which this occurs are related to the rays that would have a bottom vertex within the water column.

A comparison of normal mode and FFP predictions is provided in Figs. 9 through 14 for various frequencies. It is worthwhile to repeat that all the normal mode calculations were made with the two-layered bottom and that the FFP results are either for the same two-layered bottom or for the semi-infinite bottom. An indication of the influence of the subbottom is most evident in Fig. 9 at 25 Hz, the lowest frequency for which comparisons were attempted. In this figure, the semi-infinite bottom was used in the FFP. The agreement between the two models is good to about 40 kyd. The peak values of the normal mode solution beyond this point show a loss of about 5 dB less than their FFP counterparts. In addition, it can be seen that the two beat interference patterns are dissimilar. Some of the energy entering the two-layered bottom would be returned to the receiver after reflecting from the second bottom interface, whereas it is never returned with the semi-infinite bottom. This hypothesis was tested by including the two-layered bottom in the FFP calculations. The results of that calculation are displayed in Fig. 10. The pattern for the FFP at close ranges has the same broad features as those in the previous figure.

* Evidence of this fact is provided in Fig. 15 and will be discussed at a later point in this section.

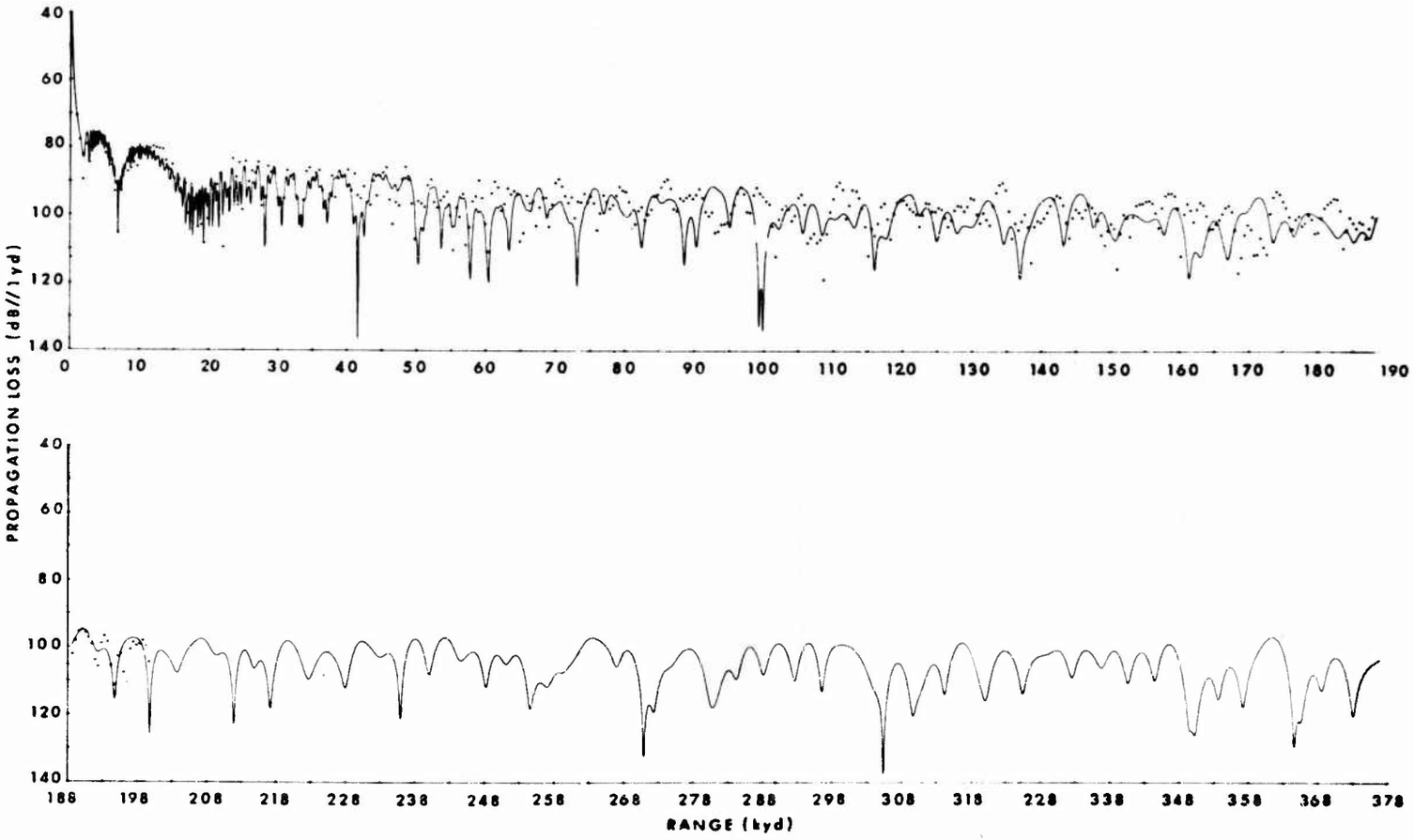

Fig. 9. FFP Propagation Loss for a Semi-infinite Bottom and a Frequency of 25 Hz

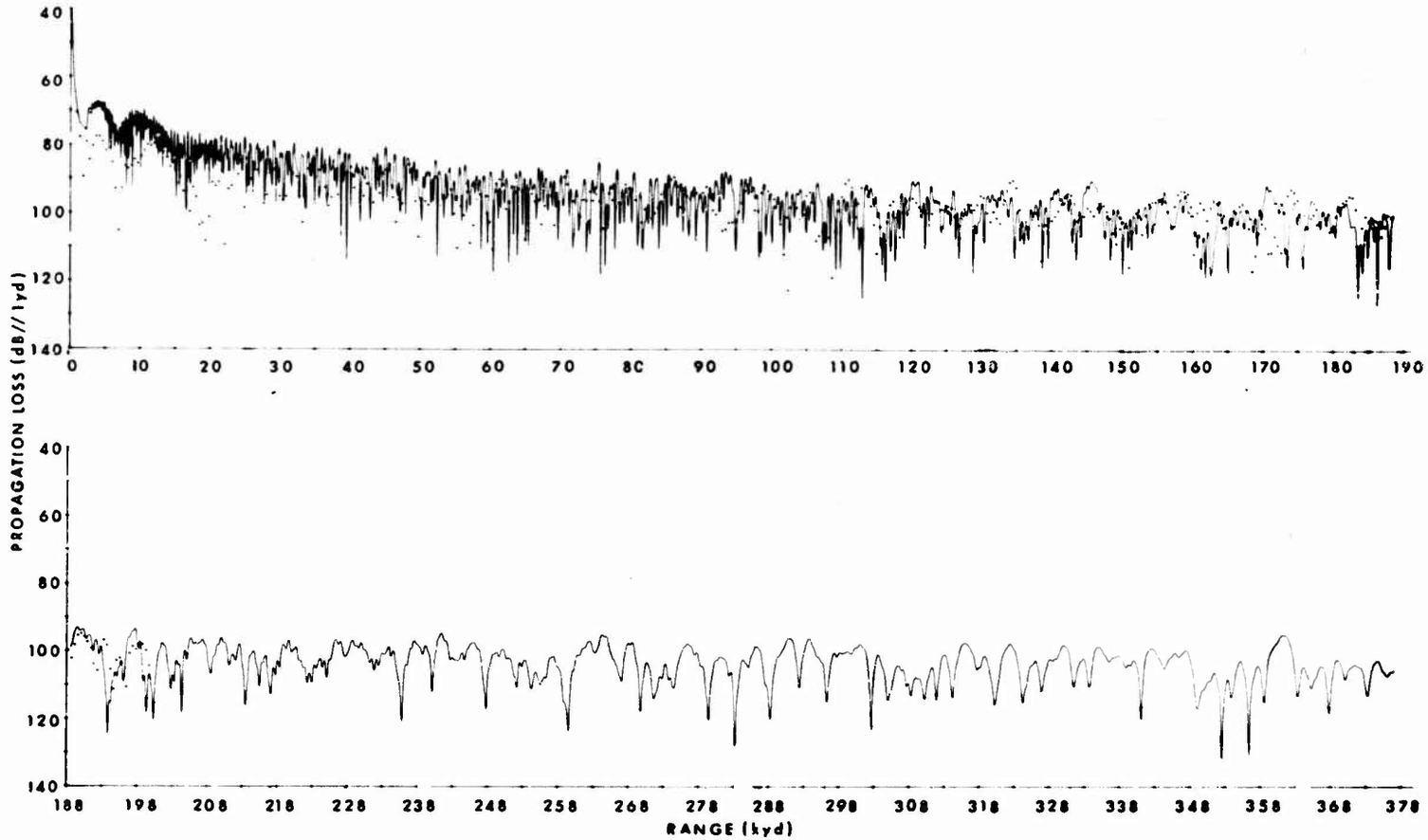

Fig. 10. FFP Propagation Loss for a Two-layered Bottom and a Frequency of 25 Hz

However, a more detailed structure is present and suggests the presence of stronger bottom arrivals. This perturbation diminishes with increasing range, a fact that could be accounted for by the decibel loss per bounce analog in ray theory. A further comparison of the two figures reveals that the peak values of both results are in better agreement.

Similar comparative runs were made at 35, 50, and 100 Hz to determine the impact of the subbottom with increasing frequency. As might be expected, the subbottom becomes less significant as the wavelength decreases. A comparison of the FFP and normal mode theory is provided in Figs. 11 and 12, at 35 and 50 Hz, respectively, for the two-layered bottom. The results at 100 Hz, with the different bottom types, are given in Figs. 13 and 14.

A comparison of these two figures reveals that at close ranges the pattern for the two-layered bottom (Fig. 13) contains a finer structure than that for the single-layered bottom. This effect is the same as that observed at 25 Hz. Since no systematic difference in level exists, however, it appears that at 100 Hz most of the energy is trapped in the water column.

Isolated ranges exist at all frequencies where the FFP and normal mode predictions are in wide disagreement. This was not the case in the single-layer comparisons of Fig. 3. It is felt that these isolated discrepancies are partially due to the omission of the phase information of the reflection coefficient in the normal mode calculations. A second difference in the two results occurs at the very close ranges where the FFP results for the two-layered bottom show substantially less loss than the normal mode results for all the frequencies presented. Explanations in terms of such things as (1) the phase of the reflection coefficient, (2) branch cut contributions, and (3) the fact that the profile varies exponentially with depth for the FFP and linearly in the normal mode program, exist but have not been substantiated.

Additional evidence of the contribution from the layered bottom is provided in Fig. 15, where the magnitude of the input at 35 Hz is plotted versus the variable of integration. The results for the semi-infinite and two-layered bottom, respectively, are plotted on alternate levels for comparative purposes. The magnitude is larger for the two-layered bottom over the entire region sampled except at the very end. The larger peaks correspond to modes associated with the bottom. The fact that the two results are almost identical for wave numbers greater than .043 is explained by means of Eq. (20); that is, in this region, $|\nu_2| > \gamma_2^3$ and the Green's function is independent of the bottom admittance.

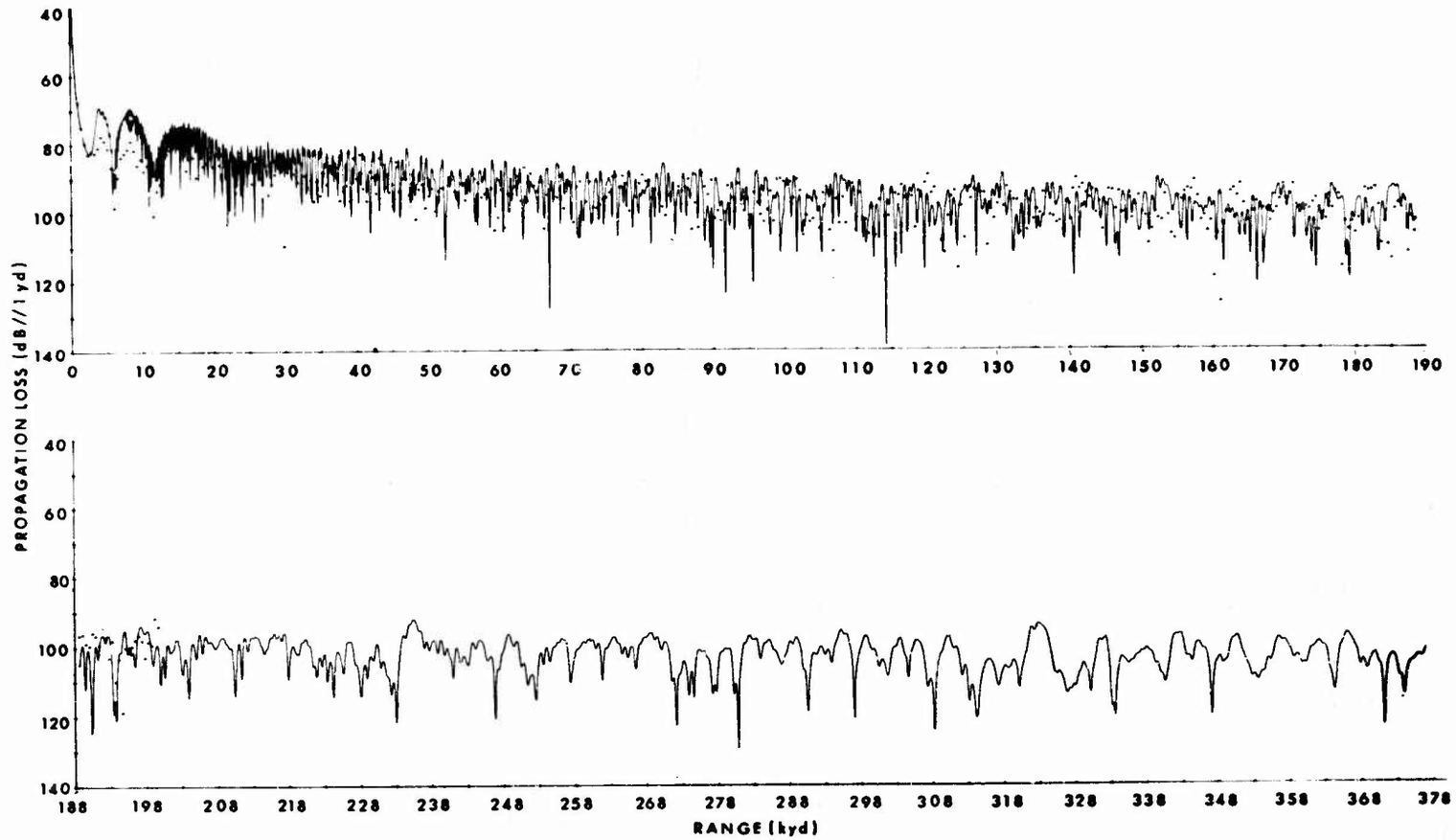

Fig. 11. FFP Propagation Loss for a Two-layered Bottom and a Frequency of 35 Hz

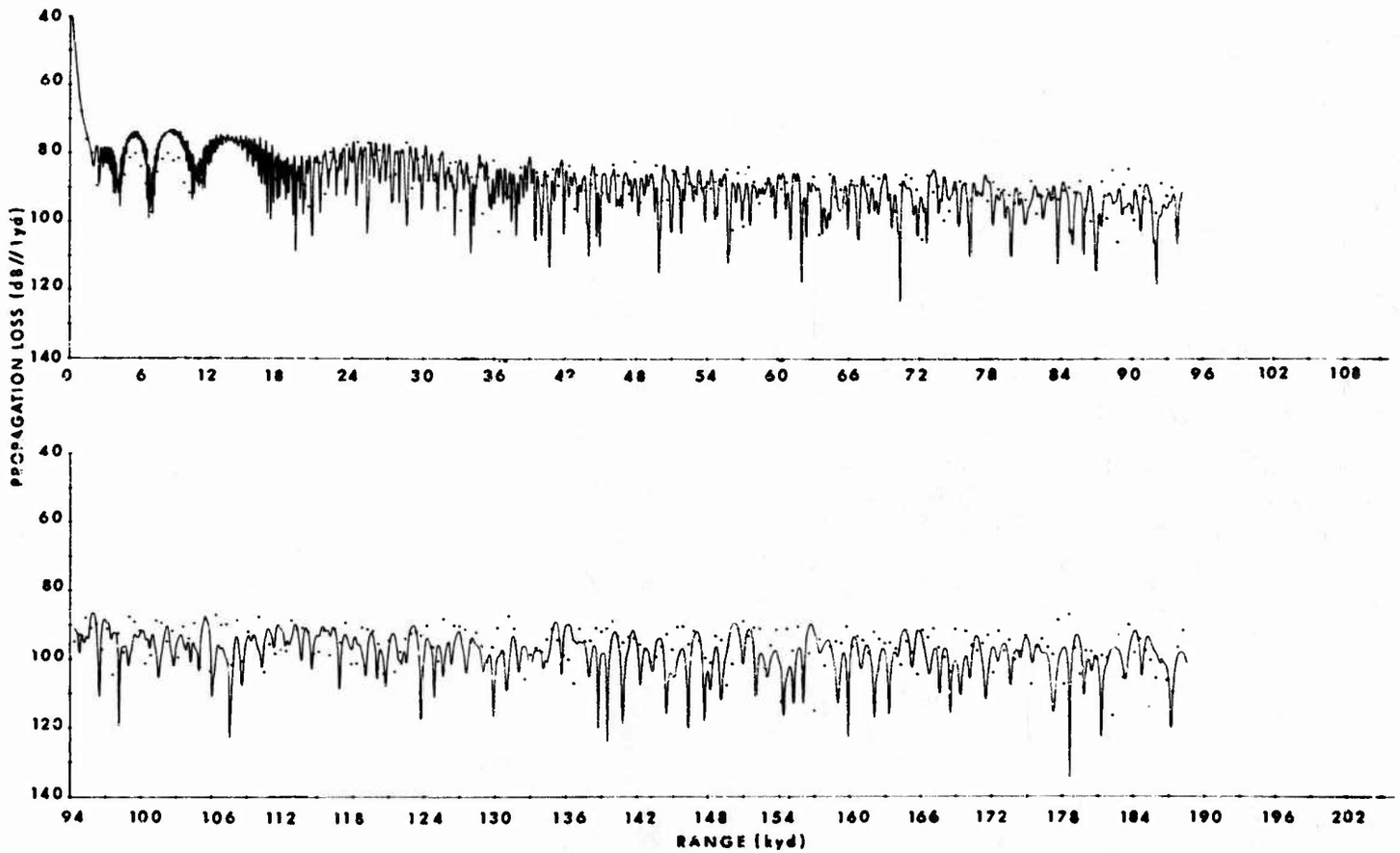

Fig. 12. FFP Propagation Loss for a Two-layered Bottom and a Frequency of 50 Hz

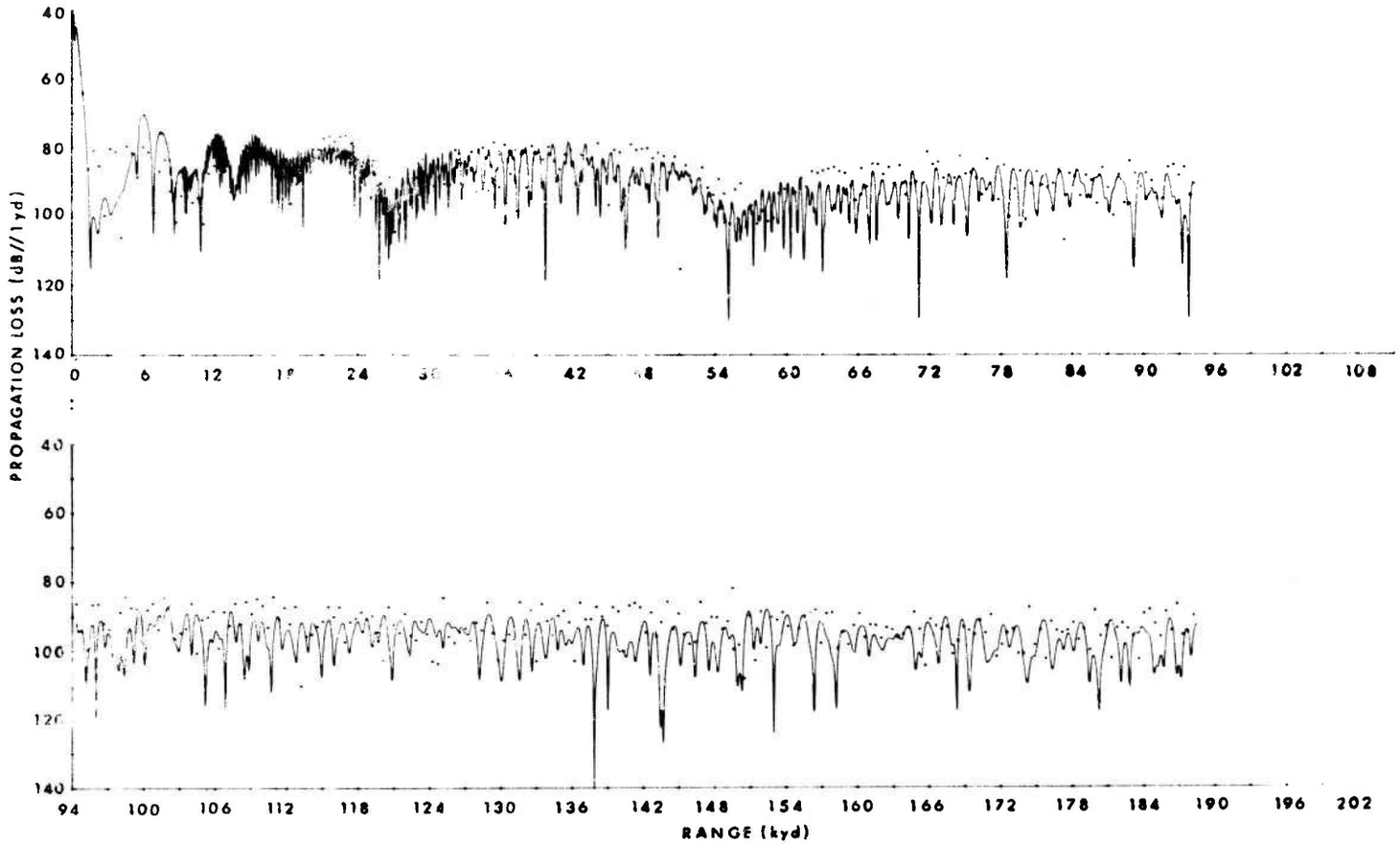

Fig. 13. FFP Propagation Loss for a Two-layered Bottom and a Frequency of 100 Hz

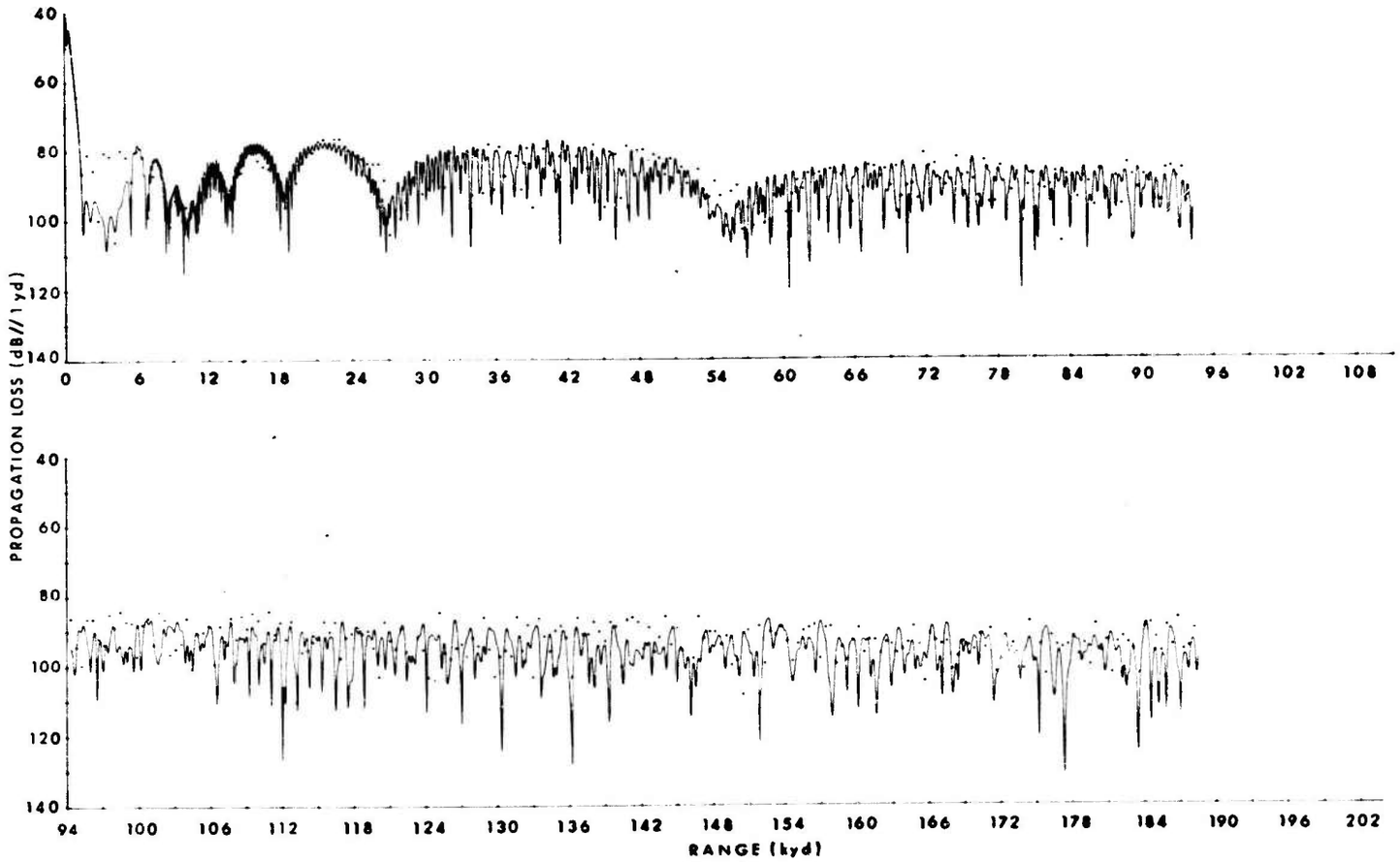

Fig. 14. FFP Propagation Loss for a Semi-infinite Bottom and a Frequency of 100 Hz

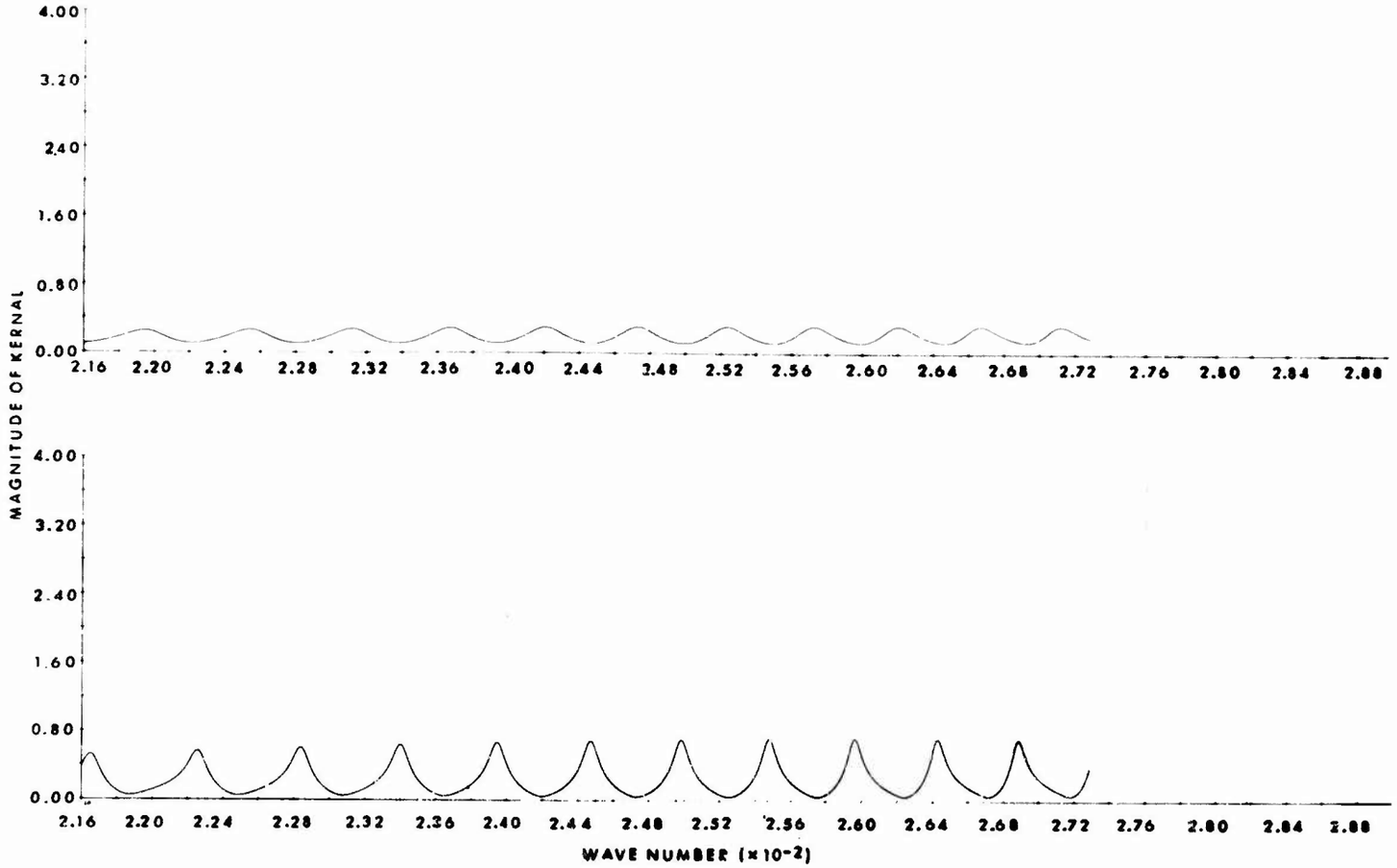

Fig. 15. Comparison of Input at 35 Hz for Different Bottom Structures

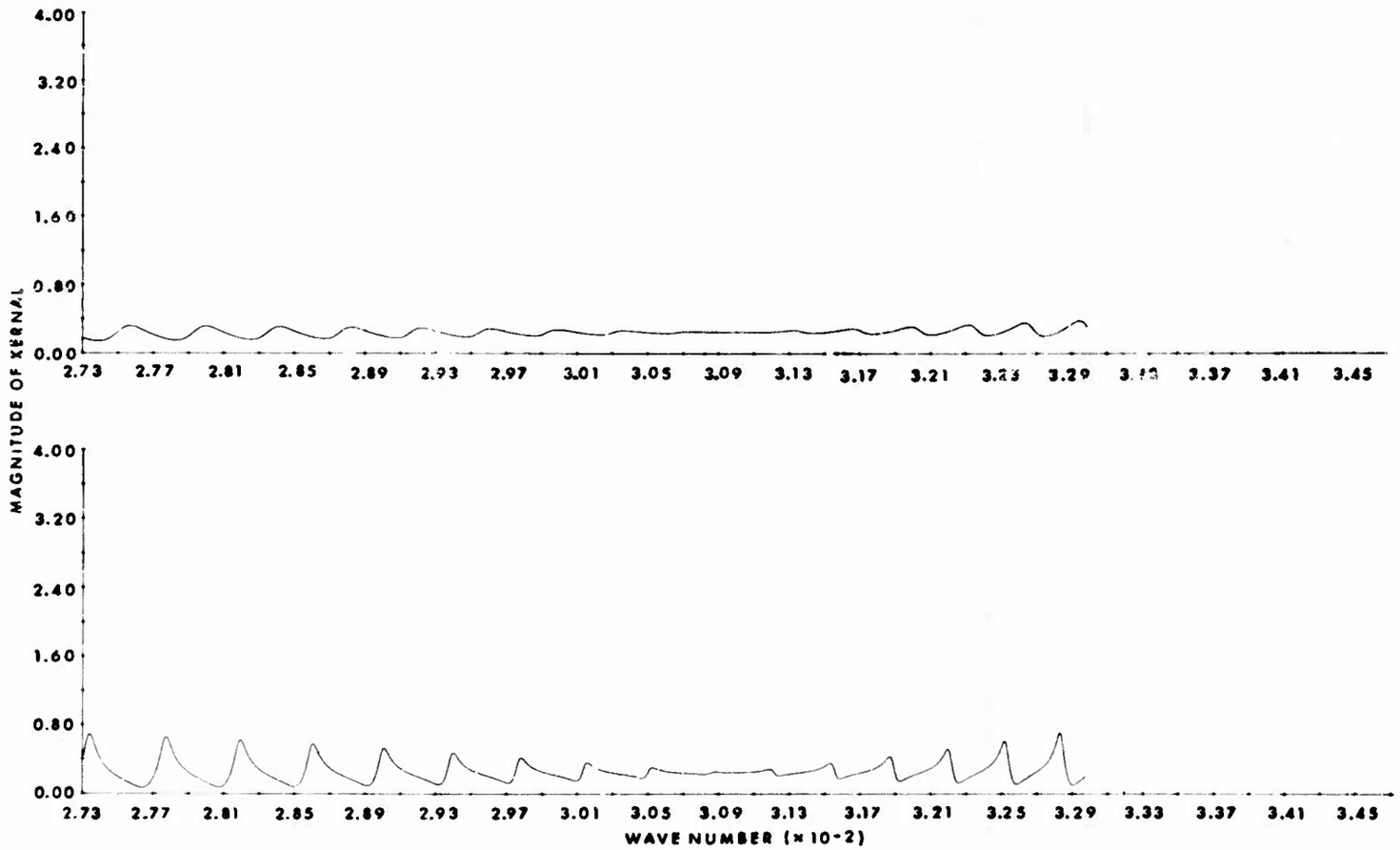

Fig. 15 (Cont'd). Comparison of Input at 35 Hz for Different Bottom Structures

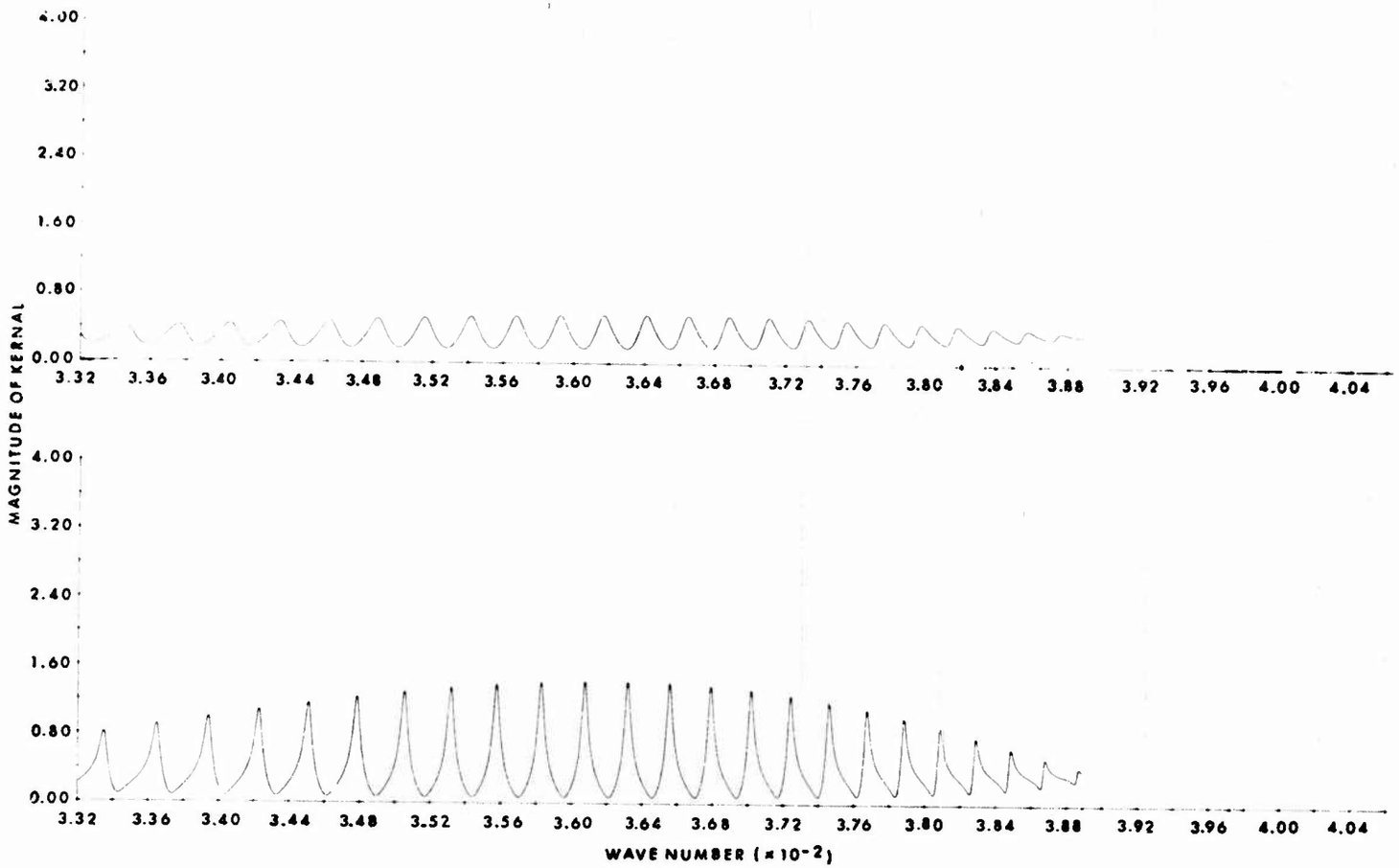

Fig. 15 (Cont'd). Comparison of Input at 35 Hz for Different Bottom Structures

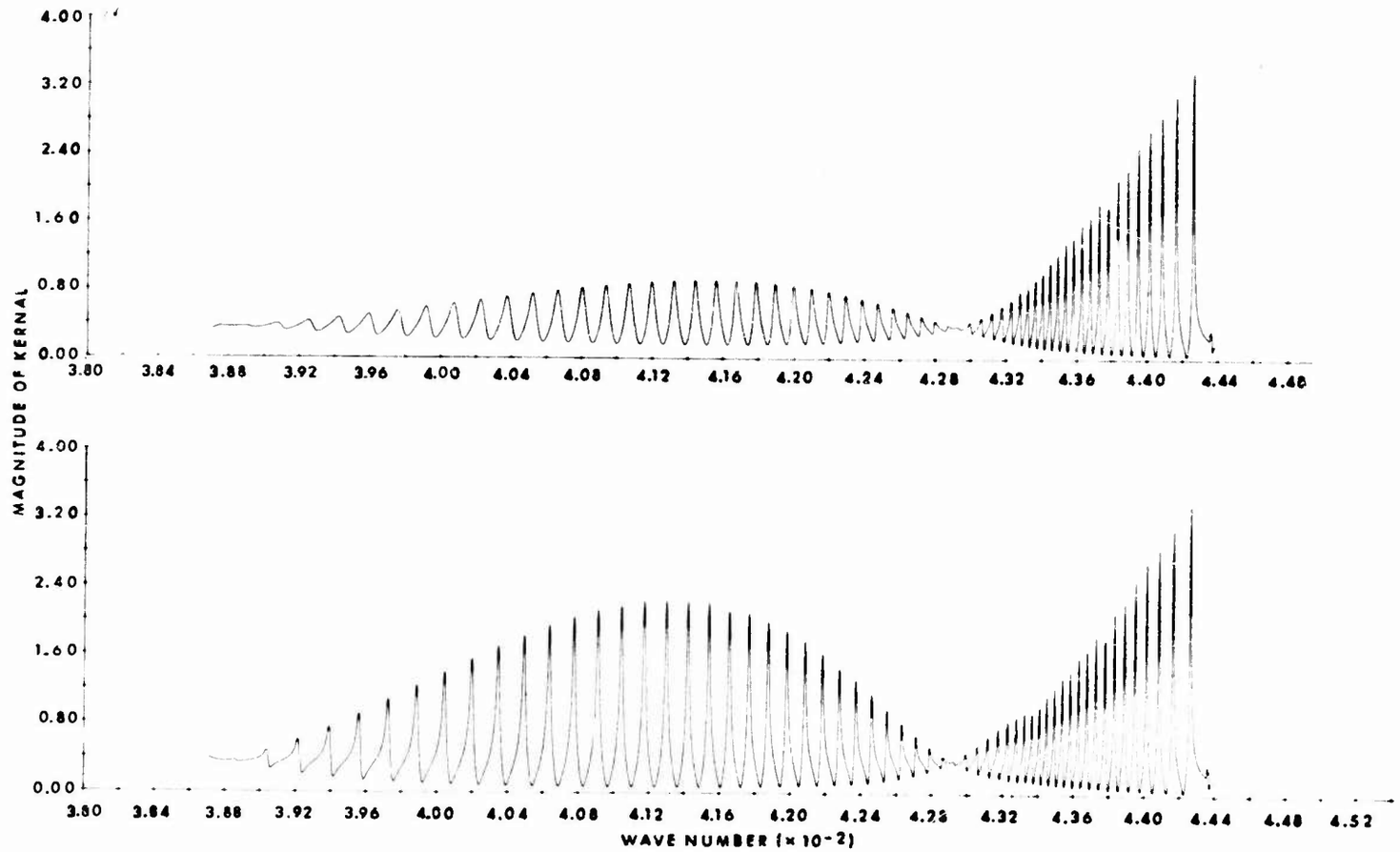

Fig. 15 (Cont'd). Comparison of Input at 35 Hz for Different Bottom Structures

An 8192 complex point FFT was used in all the above cases. The sampling distance, $\Delta\xi$, was taken as the reciprocal of H_2 at 25 and 35 Hz. At 50 and 100 Hz it was set equal to twice this value in order to provide a larger sampling region. At the lower frequencies, the FFP yields propagation loss estimations out to about 740 kyd in intervals of 92 yd. It is difficult to establish the range at which the effects of aliasing in the FFT are significant. A conservative estimate would be the midpoint, which for these examples is 180 nautical miles. For this reason, only one-half of the results have been presented in the figures in this section. The execution time for the UNIVAC 1108 was roughly 98 sec. Of this total time, 2.689 sec is required to do the FFT. Thus, the ratio of input generation time to FFT time is about 30 to 1 for this two-layer problem.

DISCUSSION

Interim results on the development of the Fast Field Program (FFP) have been reported. It is felt that the technique discussed offers a major reduction in execution time over previously investigated approaches. This has been made possible by describing the sound velocity profile in terms of an exponential variation with depth, which permits the rapid calculation of the input to the FFT through the use of recurrence relations for products of cylindrical functions.

The required execution time in utilizing this technique for a single exponential layer is the fastest possible of the various methods of input generation investigated. A more complicated environment may be accommodated via the combination of exponential layers of different gradients. The execution time increases with each additional layer, but the technique is still superior to the approaches used in the earlier development of the FFP. Along these lines it should be noted that although the ratio of generation to execution times was thirty to one for the two-layer case, the increase in time over the single-layer example was not entirely covered by the addition of a second layer. The single-layer example pertained to shallow water, whereas the two-layer model was for deep water. The water depth has a significant bearing on the total execution time, since an increase in water depth will result in a larger transition region, as discussed in the section on the Green's function, and thus will require greater computational accuracy in evaluating the kernel. This point is discussed in detail in Reference 8.

Comparisons of propagation loss predictions for the FFP and normal mode theory show that not only will the FFP provide the results quickly but also accurately. A similar comparison of execution times between these two methods

of prediction could not be made directly because the results were obtained on different computers.

In addition to demonstrating the FFP for a multilayered medium, the two-layer model also serves to illustrate the need for accurate bottom loss information at low frequencies. Inasmuch as the low-frequency end of the spectrum is attracting more attention, it would be desirable to have additional bottom loss information available.

REFERENCES

1. H. W. Marsh and S. R. Elam, Internal Document, Raytheon Company, Marine Research Laboratory, New London, Connecticut, 1967.

2. F. R. DiNapoli, Acoustic Propagation in a Stratified Medium, NUSL Report No. 1046, 13 August 1969.

3. J. W. Cooley and J. W. Tukey, "An Algorithm for the Machine Calculation of Complex Fourier Series," Mathematics of Computation, vol. 19, no. 90, 1965.

4. I. S. Gradshetyn and I. M. Ryzhik, Tables of Integrals Series and Products, Academic Press, New York, 1965, p. 1005.

5. R. Courant and D. Hilbert, Methods of Mathematical Physics, Interscience Publishers, Inc., New York, 1965, Chapter V.

6. E. T. Goodwin, "Recurrence Relations for Cross Products of Bessel Functions," Quarterly Journal Mechanics and Applied Mathematics, vol. 2, pt. 1, 1949.

7. M. Abramowitz and L. A. Stegun, Handbook of Mathematical Functions, NBS Applied Mathematics Series 55, 1964.

8. F. R. DiNapoli and M. R. Powers, "Recursive Calculation of Products of Cylindrical Functions," NUSC Technical Memorandum No. PA-83-71 (in preparation).

9. C. L. Bartberger and L. L. Ackler, Normal Mode Solutions and Computer Programs for Underwater Sound Propagation, NADC Report (in preparation).

10. O. F. Hastrup, A Detailed Analysis of Acoustic Reflectivity in the Tyrrhenian Abyssal Plain, SACLANT ASW Research Centre Report No. 145, 1969.

11. C. L. Bartberger and L. L. Ackler, private communication, 1970.